

U-SEANNET: A SIMPLE, EFFICIENT AND APPLIED U-SHAPED NETWORK FOR DIAGNOSIS OF NASAL DISEASES ON NASAL ENDOSCOPIC IMAGES

Yubiao Yue², Jun Xue³, Chao Wang³, Haihua Liang¹, Zhenzhang Li^{1,*}

¹College of Mathematics and Systems Science,

Guangdong Polytechnic Normal University, Guangzhou, China

²School of Biomedical Engineering, Guangzhou Medical University, Guangzhou, China

³School of Computer Science and Technology, Anhui University, Anhui, China

ABSTRACT

Numerous studies have affirmed that deep learning models can facilitate early diagnosis of lesions in endoscopic images. However, the lack of available datasets stymies advancements in research on nasal endoscopy, and existing models fail to strike a good trade-off between model diagnosis performance, model complexity and parameters size, rendering them unsuitable for real-world application. To bridge these gaps, we created the first large-scale nasal endoscopy dataset, named 7-NasalEID, comprising 11,352 images that contain six common nasal diseases and normal samples. Subsequently, we proposed U-SEANNet, an innovative U-shaped architecture, underpinned by depth-wise separable convolution. Moreover, to enhance its capacity for detecting nuanced discrepancies in input images, U-SEANNet employs the Global-Local Channel Feature Fusion module, enabling it to utilize salient channel features from both global and local contexts. To demonstrate U-SEANNet's potential, we benchmarked U-SEANNet against seventeen modern architectures through five-fold cross-validation. The experimental results show that U-SEANNet achieves a commendable accuracy of 93.58%. Notably, U-SEANNet's parameters size and GFLOPs are only 0.78M and 0.21, respectively. Our findings suggest U-SEANNet is the state-of-the-art model for nasal diseases diagnosis in endoscopic images.

Index Terms— Nasal Diseases, Deep Learning, Medical Diagnosis, Light-weight Network, Feature Fusion

1. INTRODUCTION

Early and accurate diagnosis of nasal diseases is crucial for improving patient's quality of life and alleviating the burden on the healthcare system[1]. In clinical settings, the predominant approach for the early diagnosis of nasal diseases involves physicians utilizing a nasal endoscope to visually in-

spect the patient's nasal cavity[2, 3]. However, due to the often very similar symptoms and nasal appearance changes caused by different nasal diseases[4], the accuracy of interpreting nasal endoscopic images heavily depends on whether the expert has rich clinical experience. This directly results in that common people from limited medical resources and economically disadvantaged families struggling to access reliable medical services, often face delay in diagnosis and misdiagnoses and then miss the best treatment opportunities. Therefore, developing a more efficient and affordable tool for early and accurate of nasal diseases holds significant clinical importance.

In recent times, burgeoning evidence demonstrates the high efficiency and economical of deep learning models, positioning them as a vanguard in endoscopic images diagnosis. In the studies of ear endoscope, Zeng et al. [5] leveraged an ensemble model based on DensNet-BC169 and DensNet-BC1615 to classify 20,542 otoscopic images into eight categories and developed a PC-based application. Chen et al. [6] employed 2,171 otoscopic images, spanning 10 diseases, to train and evaluate MobileNetV2, culminating in a mobile-centric application. Their results unveiled that their model outperforms even the discernment of seasoned otolaryngologists. Moreover, in the studies of laryngeal endoscope, You et al. [7] proposed a novel dense multiscale convolutional neural network and used a dataset of 246 laryngeal endoscope images for training and evaluation. Bhattacharjee et al. [8], on the other hand, harnessed an ensemble model founded on MobileV2, EfficientNetB0, and DenseNet121 to categorize 3,000 laryngeal endoscope images. The above researches based on endoscopic images have made significant progress. However, the realm of nasal endoscopic image diagnostics remains relatively uncharted. From our comprehensive review, there are only two related studies: Girdler et al. [2], employing ResNet152, classified 297 nasal endoscopic images into normal, nasal polyps, and inverted papilloma, achieving a diagnostic accuracy of 74.20%, on par with domain experts; Concurrently, Bi et al. [9] amassed 3,179 nasal endoscopic images, encapsulating four grades of adenoid hypertrophy,

This work was supported by the NSF of Guangdong Province (No.2022A1515011044, No.2023A1515010885), and the project of promoting research capabilities for key constructed disciplines in Guangdong Province (No.2021ZDJS028). * is corresponding author.

and subsequently proposed the MIB-Anet for image categorization, with the model’s diagnostic accuracy plateauing at 76.81%. Notwithstanding these advancements, glaring lacunae persist in the study of nasal endoscopy. Foremost among these is the dearth of extensive datasets and limited categorizations, rendering it arduous to holistically appraise the efficacy of deep learning models in nasal endoscopic image recognition—this, in turn, attenuates the model’s generalization performance. Furthermore, extant literature predominantly gravitates towards conventional model evaluation metrics, sidelining some quintessential determinants: model complexity and parameters size. Practically, these determinants gauge a model’s adaptability for integration into a diverse spectrum of computational devices, particularly those constrained by storage space and computational bandwidth, such as smartphones and low-end personal computers.

In this work, we aimed to utilize deep learning model suitable for practical setting to achieve early and accurate diagnosis of nasal diseases from nasal endoscopy images. The contributions of our work can be summarized as the following: (1) we created 7-NasaleID, the first large-scale nasal endoscopy dataset covering 6 common nasal diseases as well as normal nasal samples; (2) We proposed U-SEANNet, a novel lightweight U-architecture network based on depth-wise separable convolution. In addition, we proposed Global-Local Channel Feature Fusion module. It allows the network to make full use of the key channel features in the global and local feature maps, enabling U-SEANNet to more accurately diagnose nasal endoscopic images (3) We benchmarked U-SEANNet and the remaining 17 popular architectures via five-fold cross-validation.

2. FORMATTING YOUR PAPER

2.1. Data Source

The images used in this study were obtained from 11527 patients who sought medical care in the Otolaryngology Department of Shenzhen University Second Affiliated Hospital from 2017 to 2022. All images were got by using standard endoscopes (Matrix E2, XION GmbH, Berlin, Germany) tethered to Olympus CV-170 digital endovision camera systems (Olympus Corporation, Tokyo, Japan). To ensure the accuracy of the labels, all images were cross-validated by three experts. Here, each patient corresponds to one image and then a total of 11,527 images were collected. The specific number of images for each disease as follows: Rhinosinusitis (980, RHI), Nasopharyngeal Carcinoma (776, NC), Deviation of Nasal Septum (2338, DNS), Allergic Rhinitis (1122, AR), chronic rhinosinusitis with nasal polyps (1305, CRP), Adenoid Hypertrophy (1530, AH), and Normal (3476, Nor). All images were in JPG format with a size of 800×800×3 pixels. The research protocol of this study was approved by the Review Committee of the Second Affiliated Hospital of

Shenzhen University (Approval No: BY-EC-SOP-006-01.0-A01). The Helsinki Declaration’s tenets were scrupulously followed throughout the study to respect the rights, privacy, and anonymity of the subjects. The use of de-identified data precluded the use of informed consent. We named our dataset 7-NasaleID. **Fig.1** shows some samples of various diseases.



Fig. 1. The Samples of different types of nasal images. **a.** Adenoid Hypertrophy; **b.** Allergic Rhinitis; **c.** chronic rhinosinusitis with nasal polyps; **d.** Deviation of Nasal Septum. **e.** Nasopharyngeal Carcinoma; **f.** Normal; **g.** Rhinosinusitis.

2.2. Network Architecture

The overall framework of the U-SEANNet is shown in **Fig. 2**. The stem block first extracts initial features from the input image. Subsequently, a backbone composed of five Residual Shuffle Blocks, five MobileNetV2 blocks, and five Global-Local Channel Feature Fusion Modules further extracts the advanced features. In details, the Shuffle residual block extracts semantic information at different levels within the image and does not alter the size of the feature map, and its internal structure is largely consistent with ShuffleNetV2 Block. A straightforward difference is a residual connection is used to enhance the model’s feature reuse. MobileNetV2(MV2) Blocks performs down-sampling on the feature map and doubling the number of channels. Additionally, the third MV2 Block only expands the channels. Notably, we adopted a regularization module, DropBlock, into the middle of the network to prevent the model from overfitting the training data and improve generalization performance. To alleviate performance limitations caused by small model capacity, we proposed the Global-Local Channel Feature Fusion Module. Specifically, it first concatenates shallow and deep feature maps along the channel dimension, and then apply ECA[10](Efficient Channel Attention) to guide the network to focus on key global and local channels within the feature map. Next, utilizing point-wise convolution interactives global and local features across channels. Besides, Fhigh is added to the final output, effectively boosting the network’s performance. At the end of the network, a classical classifier is used to classify the extracted image features. Additionally, to align the model with the computational precision issues on mobile devices, all activation functions within the backbone utilize the ReLU6 activation function. Given the uniqueness of our network, we have named it U-SEANNet.

2.3. Evaluation Metrics

Here, based on the characteristics of medical images, we used Accuracy, Sensitivity, and Specificity as evaluation metrics

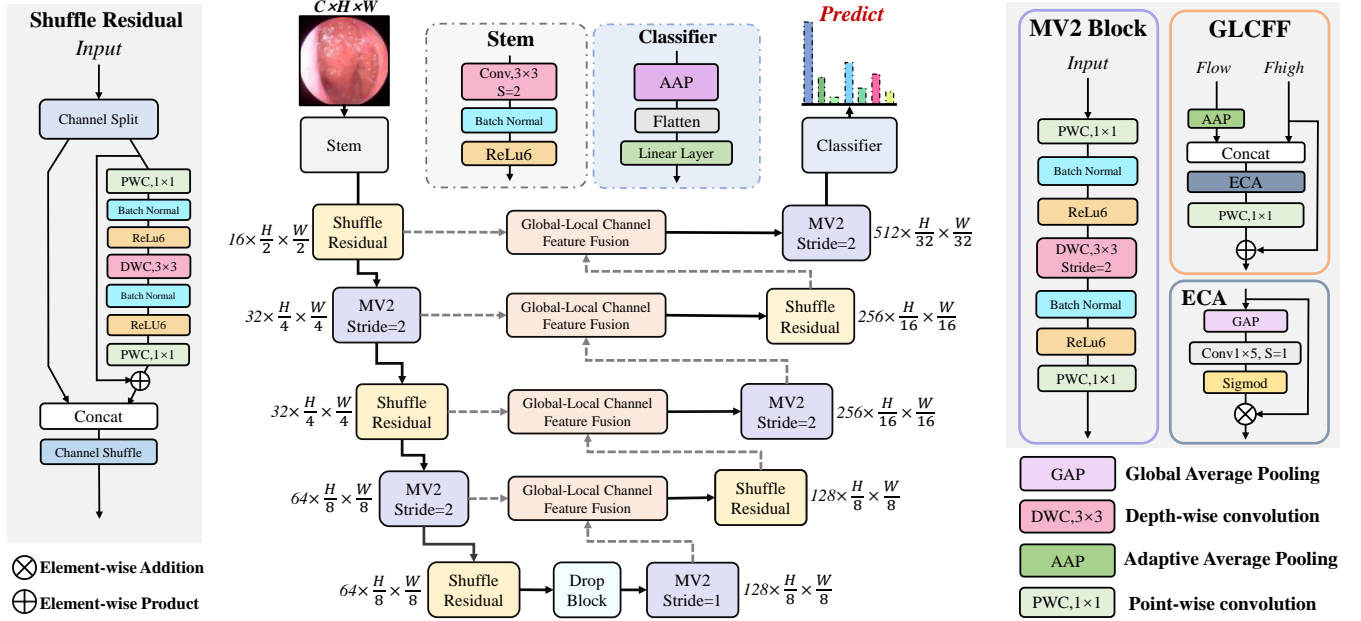


Fig. 2. The overall architecture of U-SEANNet. Here, MV2 refers to MobileNetV2 Block and Flow refers to low-level features and Fhigh refers to high-level features.

for the model. The high or low values of these three metrics can reflect the potential of the model in disease diagnosis. The definitions of these metrics are as follows:

$$Accuracy = \frac{TP + TN}{TP + TN + FP + FN} \quad (1)$$

$$Sensitivity = \frac{TP}{TP + FN} \quad (2)$$

$$Specificity = \frac{TN}{TN + FP} \quad (3)$$

In these equations, TP, TN, FP and FN are the numbers of true positives, true negatives, false positives and false negatives. In addition, we utilize GFLOPs to measure model complexity. Parameters size is calculated by Pytorch Framework.

2.4. Implementation details

In this work, the average value \pm standard deviation of the five-fold cross-validation results is used to thoroughly evaluate the potential of our network. Before training the network, we resized all images to $224 \times 224 \times 3$. Subsequently, the images were normalized and standardized using the mean $[0.8398, 0.6, 0.6263]$ and standard deviation $[0.1849, 0.28, 0.2698]$ for the three channels. During the training process, we employed the Adam optimizer with a 0.001 initial learning rate, β_1 of 0.9, β_2 of 0.999, and weight decay of $1e-4$ and Cross-Entropy Loss to optimize the model parameters. We trained the model for 150 epochs, using a batch size of 128. To train the network, we utilized the PyTorch framework, and

the training was conducted on a computer with Ubuntu 22.04 operating system and an NVIDIA GeForce RTX 4090 GPU.

3. RESULTS AND DISCUSSION

To demonstrate the potential of U-SEANNet, we chose six series of well-known networks, including both lightweight and heavyweight networks for reference. These networks are MobileNet[11, 12], EfficientNet[13], ResNet[14], DenseNet[15], MobileVit[16], and Swin Transformer[17]. Please note that the input image sizes for EfficientNet-B0 and EfficientNet-B1 are 240×240 and 260×260 , respectively, while the input size for the rest of the networks is 224×224 . All models were trained strictly according to the requirements specified in the implementation details, and unified metrics were used for evaluation.

Table 1 presents the results of U-SEANNet and other networks in terms of Accuracy, GFLOPs, and Parameters Size. Regarding accuracy, among the selected reference networks, MobileNetV2, EfficientNet-B0, ResNet50, DenseNet201, MobileVit-XXS, and Swin Transformer-Tiny achieved the best performance within their respective families, with accuracies of 91.81%, 91.40%, 92.18%, 93.25%, 91.08%, and 90.80%, respectively. In contrast, our designed U-SEANNet achieved state-of-the-art results among all the networks, with an accuracy of 93.58%. Compared to the reference networks, U-SEANNet outperformed them by 1.77%, 2.18%, 1.40%, 0.33%, 2.50%, and 2.78% in accuracy, respectively. Meanwhile, U-SEANNet demonstrated the lowest GFLOPs and Parameters Size among all the networks, with values of

Table 1. Accuracy, GFLOPs and Parameters Size (Paras Size) of U-SEANNet and other reference networks.

Model	Accuracy	GFLOPs	Paras Size
MobileNetV2	91.81%(±0.67)	0.32	2.23M
MobileNetV3-Large	91.79%(±0.58)	0.23	4.21M
EfficientNet-B0	91.40%(±0.21)	0.4	4.02M
EfficientNet-B1	90.88%(±0.23)	0.71	6.52M
EfficientNet-B2	90.89%(±0.48)	1.03	7.71M
ResNet50	92.18%(±0.40)	4.12	23.52M
ResNet101	92.01%(±0.31)	7.84	42.51M
ResNet152	91.76%(±0.51)	11.57	58.16M
DenseNet121	93.24%(±0.43)	2.88	6.96M
DenseNet161	92.97%(±0.40)	7.82	26.49M
DenseNet201	93.25%(±0.45)	4.37	18.11M
MobileVit-S	81.96%(±2.43)	1.44	4.94M
MobileVit-XS	90.85%(±0.40)	0.72	1.94M
MobileVit-XXS	91.08%(±0.22)	0.26	0.95M
SwinTransformer-T	90.80%(±0.54)	2.97	27.52M
SwinTransformer-S	90.11%(±0.51)	5.75	48.84M
SwinTransformer-B	89.15%(±0.29)	10.21	86.75M
U-SEANNet(Ours)	93.58%(±0.42)	0.21	0.78M

only 0.21 and 0.78M, respectively. Compared to the heavy-weight networks, such as ResNet50, DenseNet201, and Swin Transformer-Tiny, U-SEANNet achieved higher accuracy while significantly reducing GFLOPs by 94.9%, 95.2%, and 92.9%, and parameters size by only 3.3%, 4.3%, and 2.8% of their respective values. The experimental results clearly indicate that our work not only guarantees high accuracy in the network but also achieves remarkable lightweight characteristics, providing significant advantages for practical applications.

Next, in order to further analyze the potential of U-SEANNet in each disease diagnosis, we summarized the Sensitivity and Specificity of the networks for the 7 types of nasal images in **Table 2**. For reference we also reported the results of the best-performing network among various series of networks. As shown in Table 2, U-SEANNet achieved the highest Sensitivity in four categories: AR, DNS, NC, and RHI, with respective scores of 77.28%, 93.93%, 99.87%, and 96.74%. Similarly, U-SEANNet achieved the best performance in Specificity for the AH, CRP, NOR, and RHI categories, with results of 99.81%, 99.42%, 96.68%, and 99.39%, respectively.

The experimental results demonstrate that, through a comprehensive analysis of Accuracy, GFLOPs, Parameters Size, Sensitivity, and Specificity, our network not only exhibits the best potential for diagnosing nasal diseases but also facilitates practical application.

4. CONCLUSION

This paper proposed a simple, efficient and applied network for diagnosing nasal diseases. Our network not only is far

Table 2. The Sensitivity and Specificity of various networks for the seven types of diseases.

Model	Diseases	Sensitivity	Specificity
U-SEANNet(Ours)	AH	98.23%(±0.67)	99.81%(±0.07)
	AR	77.28%(±3.25)	98.52%(±0.23)
	CRP	92.18%(±0.90)	99.42%(±0.33)
	DNS	93.93%(±1.00)	98.82%(±0.38)
	NC	99.87%(±0.26)	99.82%(±0.11)
	NOR	94.79%(±1.01)	96.68%(±0.37)
MobileNetV2	RHI	96.74%(±1.39)	99.39%(±0.13)
	AH	97.84%(±0.89)	99.61%(±0.02)
	AR	74.61%(±3.23)	97.64%(±0.82)
	CRP	89.89%(±3.89)	99.06%(±0.21)
	DNS	90.72%(±0.92)	98.59%(±0.64)
	NC	99.48%(±0.48)	99.81%(±0.12)
EfficientNet-B0	NOR	93.70%(±1.88)	96.30%(±0.62)
	RHI	94.49%(±2.10)	98.91%(±0.36)
	AH	98.23%(±0.44)	99.55%(±0.15)
	AR	71.30%(±6.03)	98.10%(±0.41)
	CRP	88.51%(±2.94)	99.01%(±0.22)
	DNS	92.43%(±1.20)	97.87%(±0.69)
ResNet50	NC	98.58%(±1.70)	99.74%(±0.19)
	NOR	93.44%(±1.64)	96.11%(±0.51)
	RHI	92.25%(±1.49)	98.97%(±0.42)
	AH	98.24%(±0.94)	99.71%(±0.17)
	AR	70.58%(±6.13)	98.28%(±0.20)
	CRP	90.19%(±1.98)	99.17%(±0.28)
DenseNet201	DNS	91.58%(±3.36)	98.52%(±0.59)
	NC	99.48%(±1.03)	99.82%(±0.14)
	NOR	94.97%(±1.82)	95.63%(±0.69)
	RHI	95.92%(±1.41)	99.04%(±0.29)
	AH	98.89%(±0.96)	99.73%(±0.15)
	AR	74.33%(±3.53)	98.58%(±0.19)
MobileVit-XXS	CRP	93.33%(±2.68)	99.04%(±0.22)
	DNS	93.89%(±2.06)	98.38%(±0.39)
	NC	99.61%(±0.32)	99.88%(±0.10)
	NOR	94.48%(±1.10)	96.60%(±0.60)
	RHI	95.10%(±2.97)	99.35%(±0.15)
	AH	98.37%(±0.68)	99.50%(±0.31)
SwinT-T	AR	72.46%(±5.70)	97.48%(±0.57)
	CRP	86.74%(±2.28)	99.15%(±0.19)
	DNS	91.32%(±1.72)	98.34%(±0.38)
	NC	98.58%(±0.75)	99.73%(±0.10)
	NOR	93.35%(±1.00)	95.80%(±0.66)
	RHI	92.15%(±2.47)	98.96%(±0.17)
	AH	97.91%(±0.44)	99.53%(±0.23)
	AR	70.50%(±4.21)	97.50%(±0.22)
	CRP	85.44%(±3.30)	99.05%(±0.29)
	DNS	91.58%(±2.07)	98.08%(±0.32)
	NC	98.32%(±1.85)	99.68%(±0.10)
	NOR	93.15%(±0.86)	96.09%(±0.81)
	RHI	93.98%(±2.98)	98.76%(±0.31)

ahead of various modern architectures in terms of Accuracy but also exhibits extremely low GFLOPs and Parameters Size. The next step in our work is to address the issue of imbalanced datasets. It is evident that due to the insufficient sample size for AR and CRP, the diagnostic capabilities of these two diseases are slightly inferior. Additionally, we will further test our model on diverse populations and develop the specific application. We also plan to conduct human-machine comparative studies, which will help evaluate the model's performance in real-world settings with the participation of human expertise, thereby enhancing its overall utility and applicability.

5. REFERENCES

- [1] Wen Wen, Shi-Juan Mai, Huan-Xin Lin, Mei-Yin Zhang, Jia-Ling Huang, Xin Hua, Chao Lin, Zhi-Qing Long, Zi-Jian Lu, Xiao-Qing Sun, et al., “Identification of two microrna signatures in whole blood as novel biomarkers for diagnosis of nasopharyngeal carcinoma,” *Journal of translational medicine*, vol. 17, pp. 1–13, 2019.
- [2] Benton Girdler, Hyun Moon, Mi Rye Bae, Sung Seok Ryu, Jihye Bae, and Myeong Sang Yu, “Feasibility of a deep learning-based algorithm for automated detection and classification of nasal polyps and inverted papillomas on nasal endoscopic images,” in *International Forum of Allergy & Rhinology*. Wiley Online Library, 2021, vol. 11, pp. 1637–1646.
- [3] Y K Maru and Y Gupta, “Nasal endoscopy versus other diagnostic tools in sinonasal diseases,” *Indian Journal of Otolaryngology and Head & Neck Surgery*, vol. 68, pp. 202–206, 2016.
- [4] Utku Aydil, Hande Karadeniz, and Caner Şahin, “Choanal polyp originated from the inferior nasal concha,” *European archives of oto-rhino-laryngology*, vol. 265, no. 4, pp. 477–479, 2008.
- [5] Xinyu Zeng, Zifan Jiang, Wen Luo, Honggui Li, Hongye Li, Guo Li, Jingyong Shi, Kangjie Wu, Tong Liu, Xing Lin, et al., “Efficient and accurate identification of ear diseases using an ensemble deep learning model,” *Scientific Reports*, vol. 11, no. 1, pp. 10839, 2021.
- [6] Yen-Chi Chen, Yuan-Chia Chu, Chii-Yuan Huang, Yen-Ting Lee, Wen-Ya Lee, Chien-Yeh Hsu, Albert C Yang, Wen-Huei Liao, and Yen-Fu Cheng, “Smartphone-based artificial intelligence using a transfer learning algorithm for the detection and diagnosis of middle ear diseases: A retrospective deep learning study,” *EClinicalMedicine*, vol. 51, 2022.
- [7] Zhenzhen You, Yan Yan, Zhenghao Shi, Minghua Zhao, Jing Yan, Haiqin Liu, Xinhong Hei, and Xiaoyong Ren, “Laryngeal leukoplakia classification via dense multi-scale feature extraction in white light endoscopy images,” in *ICASSP 2023-2023 IEEE International Conference on Acoustics, Speech and Signal Processing (ICASSP)*. IEEE, 2023, pp. 1–5.
- [8] Ramanuj Bhattacharjee, K Suganya Devi, and S Vijaykanth, “Detecting laryngeal cancer lesions from endoscopy images using deep ensemble model,” in *2023 International Conference on Signal Processing, Computation, Electronics, Power and Telecommunication (IConSCEPT)*. IEEE, 2023, pp. 1–6.
- [9] Mingmin Bi, Siting Zheng, Xuechen Li, Haiyan Liu, Xiaoshan Feng, Yunping Fan, and Linlin Shen, “Mib-anet: A novel multi-scale deep network for nasal endoscopy-based adenoid hypertrophy grading,” *Frontiers in Medicine*, vol. 10, pp. 1142261, 2023.
- [10] Qilong Wang, Banggu Wu, Pengfei Zhu, Peihua Li, Wangmeng Zuo, and Qinghua Hu, “Eca-net: Efficient channel attention for deep convolutional neural networks,” in *Proceedings of the IEEE/CVF conference on computer vision and pattern recognition*, 2020, pp. 11534–11542.
- [11] Andrew G Howard, Menglong Zhu, Bo Chen, Dmitry Kalenichenko, Weijun Wang, Tobias Weyand, Marco Andreetto, and Hartwig Adam, “Mobilenets: Efficient convolutional neural networks for mobile vision applications,” *arXiv preprint arXiv:1704.04861*, 2017.
- [12] Andrew Howard, Mark Sandler, Grace Chu, Liang-Chieh Chen, Bo Chen, Mingxing Tan, Weijun Wang, Yukun Zhu, Ruoming Pang, Vijay Vasudevan, et al., “Searching for mobilenetv3,” in *Proceedings of the IEEE/CVF international conference on computer vision*, 2019, pp. 1314–1324.
- [13] Mingxing Tan and Quoc Le, “Efficientnet: Rethinking model scaling for convolutional neural networks,” in *International conference on machine learning*. PMLR, 2019, pp. 6105–6114.
- [14] Kaiming He, Xiangyu Zhang, Shaoqing Ren, and Jian Sun, “Deep residual learning for image recognition,” in *Proceedings of the IEEE conference on computer vision and pattern recognition*, 2016, pp. 770–778.
- [15] Gao Huang, Zhuang Liu, Laurens Van Der Maaten, and Kilian Q Weinberger, “Densely connected convolutional networks,” in *Proceedings of the IEEE conference on computer vision and pattern recognition*, 2017, pp. 4700–4708.
- [16] Sachin Mehta and Mohammad Rastegari, “Mobilevit: light-weight, general-purpose, and mobile-friendly vision transformer,” *arXiv preprint arXiv:2110.02178*, 2021.
- [17] Ze Liu, Yutong Lin, Yue Cao, Han Hu, Yixuan Wei, Zheng Zhang, Stephen Lin, and Baining Guo, “Swin transformer: Hierarchical vision transformer using shifted windows,” in *Proceedings of the IEEE/CVF international conference on computer vision*, 2021, pp. 10012–10022.